Food and Chemical Toxicology 123 (2019) 258–267

Contents lists available at ScienceDirect

Food and Chemical Toxicology

journal homepage: www.elsevier.com/locate/foodchemtox

Assessing the relevance of exposure time in differentiated Caco-2/HT29 cocultures. Effects of silver nanoparticles

Miriam Saez-Tenorio[a,1], Josefa Domenech[a,1], Alba García-Rodríguez[a], Antonia Velázquez[a,b], Alba Hernández[a,b], Ricard Marcos[a,b,**], Constanza Cortés[a,*]

[a] Grup de Mutagènesi, Departament de Genètica i de Microbiologia, Facultat de Biociències, Universitat Autònoma de Barcelona, Bellaterra, Spain
[b] Consortium for Biomedical Research in Epidemiology and Public Health (CIBERESP), Carlos III Institute of Health, Madrid, Spain

ARTICLE INFO

Keywords:
Silver nanoparticles
Caco-2/HT29 cocultures
Exposure time
Barrier integrity
Uptake
Translocation

ABSTRACT

In vitro models of the intestinal barrier are being increasingly used to evaluate nanoparticles (NPs) exposure risk. Nevertheless, most of these studies have focused on short-term exposures lasting no more than 24 h of duration, which could underestimate the toxic effects of a given compound under a more realistic setting. Since the assessment of longer exposure time-points is crucial to evaluate the risk of cumulative exposure to NPs, we have analyzed the effects of AgNPs at different exposure time-points between 6 h and 4 days on the barrier model system constituted by Caco-2/HT29 cells.

Our results indicate that i) the system is stable during this time frame; ii) AgNPs affect the barrier's integrity only at the highest concentration tested (100 μg/mL), and only after 96 h of exposure; iii) cellular uptake of AgNPs showed a time-dependent and concentration-dependent increase; iv) translocation through the barrier was only observed at the highest concentration and only after 96 h of exposure; v) the expression of genes involved in the barrier's structure differs depending on the exposure time analyzed.

All these results reinforce our proposal of expanding exposure times beyond 24 h when performing assays for hazard assessment of NPs using *in vitro* models of the intestinal barrier.

1. Introduction

Ingestion is one of the main routes by which nanoparticles (NPs) can enter the body (Sahu, 2016). Given the importance of the gastrointestinal barrier (GIB) as an interface between living organisms and the external environment, several models are being used to study the putative detrimental effects of ingested agents over the barrier's function and permeability. Currently, risk assessment mostly relies on *in vivo* animal models, mainly due to the advantage of providing toxicokinetic information. Nonetheless, the reduction of animal studies is strongly promoted by the scientific community for numerous reasons, such as ethical concerns, or the lack of correspondence with human physiology and metabolism (Scholz et al., 2013). Consequently, the development of reliable human *in vitro* models of the GIB has been prompted in order to better understand the cellular and molecular aspects of hazardous ingested substances, which at the same time provide a faster and more economical alternative to animal models.

One of the most commonly used *in vitro* systems for toxicological studies is the Caco-2 monolayer barrier (Lefebvre et al., 2015). This cell line, derived from a human colon adenocarcinoma, is highly popular due to its capability to undergo cellular differentiation. When cultured under specific conditions, Caco-2 cells form a polarized monolayer, which mimics the morphological, functional and biochemical characteristics of enterocytes (Halleux and Schneider, 1991; Levy et al., 1995; Vila et al., 2018). When this monolayer is grown on a porous membrane, two cellular compartments are formed, the apical compartment that simulates the intestinal lumen and the basal compartment simulating the *lamina propia*. The resulting cell monolayer presents high stability and integrity, forming a barrier that provides selective permeability from the apical to the basolateral compartment, especially due to the expression of junctional complex proteins. Several studies have demonstrated the usefulness of the Caco-2 barrier model in

* Corresponding author. Grup de Mutagènesi, Departament de Genètica i de Microbiologia, Universitat Autònoma de Barcelona, Edifici Cn, Campus de Bellaterra, 08193, Cerdanyola del Vallès, Barcelona, Spain.
** Corresponding author. Grup de Mutagènesi, Departament de Genètica i de Microbiologia, Universitat Autònoma de Barcelona, Edifici Cn, Campus de Bellaterra, 08193, Cerdanyola del Vallès, Barcelona, Spain.
E-mail addresses: ricard.marcos@uab.es (R. Marcos), constanza.cortes@uab.es (C. Cortés).
[1] Both persons contributed equally to the work.

https://doi.org/10.1016/j.fct.2018.11.009
Received 22 September 2018; Received in revised form 30 October 2018; Accepted 3 November 2018
Available online 04 November 2018
0278-6915/

predicting the effects of different xenobiotics, such as drugs or NPs, over the human GIB, as the barrier presents a different response to cytotoxicity when compared to single cell cultures (Sun et al., 2008; Vila et al., 2018; Sohal et al., 2018). However, the intestinal epithelium is a complex environment comprising multiple cell types, making the monolayer of Caco-2 cells not accurate enough for hazard assessment of potentially toxic substances (Hidalgo, 1996). As a more complete alternative, mucin-secreting cells, such as the human colon adenocarcinoma-derived HT29 or HT29/MTX cell lines, have been cocultured with Caco-2 cells. It is widely accepted that the mucus layer secreted by goblet cells in the gastrointestinal tract serves as an additional physical defence against potentially damaging agents such as chemicals, microbiota, and host-secreted products such as bile and digestive enzymes (Pontier et al., 2001; Johansson et al., 2008). Furthermore, HT29 cells do not form tight junctions. Thus, the combined presence of enterocyte-like and mucus-secreting cell types better simulates the GIB by adding an extra protection layer while increasing its permeability (García-Rodriguez et al., 2018).

Of all the known ingested nanomaterials, silver nanoparticles (AgNPs) have gained particular attention due to their extended use in the food industry, and their confirmed migration from packaging to food (Echegoyen and Nerín, 2013; McShan et al., 2014). The ingestion throughout the day of AgNP-containing edible goods implies a continuous exposure to these NPs, but their long-term effects over the human GIB has not been elucidated yet. Animal models have led to contrasting results, probably due to differences in the experimental design and the physiology of the animals used (Fontdevila et al., 2008; Shahare and Yashpal, 2013). When it comes to the human-derived Caco-2 and Caco-2/HT29 monolayer models, previous studies demonstrate that AgNPs do not destabilize the barrier, although effects such as NPs intake, activation of the inflammatory response, oxidative damage and genetic and protein destabilization have been observed (Georgantzopoulou et al., 2016; Martirosyan et al., 2016; Vila et al., 2018). Most of these studies have focused in short-term toxicological analyses usually lasting for less than 24 h that, albeit informative, could be underestimating the toxic effects of longer and constant accumulative exposures. It has been previously shown that the mucus layer traps metallic NPs, favouring their accumulation in the underlying cell barrier (Brun et al., 2014). As mucus turnover in the intestine can range between 3 and 12 h (Schneider et al., 2018), the ingestion throughout the day of AgNPs could extend the NPs' retention time in certain regions of the intestine long enough to present cumulative effects. Longer-term analyses would, therefore, correspond to a more realistic scenario, better emulating the sustained stress suffered by the GIB in response to regular exposure. In fact, several studies using different models have demonstrated the utility of prolonging exposure times, as continuous contact with NPs can induce cumulative effects such as ROS formation or cell transformation markers (Annangi et al., 2015). On the contrary, an initial damage response could be mitigated over time, as cells activate damage-response mechanisms and develop resistance to nanomaterials (Iavicoli et al., 2018). Therefore, the development of models that faithfully simulate the GIB environment, while faithfully assessing the effect of NPs' interaction over longer periods of time is crucial for unravelling the real effects of continuous exposure to these xenobiotic compounds.

In this context, the objective of our work was to validate the Caco-2/HT29 coculture barrier as a suitable model for exposure studies longer than 24 h. We further tested the system to see whether the exposure to AgNPs shows variations over a 96 h exposure. To this aim, we analyzed the stability, permeability and molecular marker expression of the barrier over time, as well as the translocation and localization of the AgNPs throughout the exposure time.

2. Materials and methods

2.1. AgNPs dispersion and characterization

Uncoated AgNPs were obtained from Nanocomposix (Prague, Czech Republic). To disperse them, we followed the protocol agreed in the frame of the EU project Nanogenotox (2011). Briefly, AgNPs were suspended in 0.05% bovine serum albumin (BSA) in MilliQ water and sonicated for 16 min to obtain a dispersed stock of 2.56 mg/mL. AgNPs were further characterized by using transmission electron microscopy (TEM) to determine the nanoparticle's dried size and morphology, on a JEOL JEM-1400 instrument (Jeol LTD, Tokyo, Japan). About 100 TEM images from random fields of view were processed with Image J software to calculate their average diameter. Additionally, hydrodynamic size and Z-potential parameters were evaluated using dynamic light scattering (DLS) and laser Doppler velocimetry (LDV) methodologies, in a Malvern ZetasizerNano-ZS zen3600 device (Malvern, UK).

2.2. Cell culture and reagents

Two different cell lines derived from human colorectal adenocarcinoma were used: the Caco-2 cell line was kindly provided by Dr Isabella Angelis (Istituto Superiore di Sanità, Italy); HT29 cells were acquired from the American Type Culture Collection (ATCC, Manassas VA 20108, USA). Both cell lines were maintained in Dulbecco's modified Eagle's High Glucose medium (DMEM) without pyruvate (Biowest, France) supplemented with 10% fetal bovine serum (FBS), 1% non-essential amino acids (NEAA) (Biowest, France) and 2.5 mg/mL plasmocin (Invivo Gen, San Diego, CA). Cells were grown in a humidified atmosphere of 5% CO_2 and 95% air, at 37 °C. For cell culture maintenance, cells were routinely subcultured thrice a week at 80% confluence by treatment with 1% trypsin–EDTA (Biowest, France).

2.3. Differentiation of the in vitro coculture barrier model

Caco-2 and HT29 cells were seeded at a ratio of 90:10, respectively, on 1.12 cm^2 Polyethylene Terephthalate (PET) Transwell® membranes with 1 μm pores (Merck KGaA, Darmstadt, Germany) inside 12-well plates (García-Rodriguez et al., 2018). A total of 1.7×10^5 cells were seeded per Transwell® and grown for 21 days to obtain the well-differentiated coculture barrier. The integrity of the coculture monolayer was controlled weekly by measuring the transepithelial electrical resistance (TEER) every week, during the differentiation period.

2.4. TEER measurements

The barrier model's formation and integrity were evaluated by measuring its transepithelial electrical resistance (TEER). Measurements were performed on cell cocultures using an epithelial voltmeter (Millicell-ERS volt/ohm meter) (Millipore) (Merck KGaA, Darmstadt, Germany). To monitor the barrier's formation, TEER was measured weekly from day 7 to day 21 post-seeding to assess differentiation. TEER values higher than 300 Ω/cm^2 were considered indicative of a well-formed barrier, according to the acceptance criteria reported on ECVAM DB-ALM Protocol n.142 (Le Ferrec et al., 2001).

To assess the effects of AgNPs on the barrier's integrity, the apical and basolateral chambers were washed thrice with phosphate buffer saline (PBS) after 6, 24, 48 or 96 h of exposure. Fresh DMEM cell culture medium was subsequently added to both chambers, and each sample was measured two times in different parts of the insert before and after AgNPs exposure. TEER values for each concentration were calculated by averaging three independent experiments. TEER values were calculated according to the formula TEER = [Ω (cell inserts) – Ω (cell-free inserts)] x 1.12 cm^2.

A

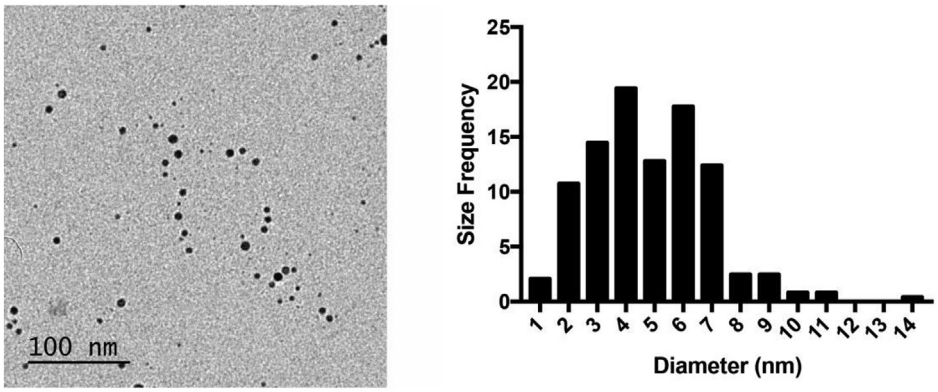

B

DLS		LDV	
Polydispersity Index (PDI)	Average hydrodynamic size (nm)	Z-potential ζ (mV)	Electrophoretic mobility (μm·cm/V·s)
0.495 ± 0.014	9.720 ± 1.571	-20.14 ± 0.611	-1.602 ± 0.048

Fig. 1. Characterization of AgNPs. (A) Typical TEM image, and size distribution histogram using such images. (B) Different parameters on AgNPs dispersed in the suspension medium.

2.5. AgNPs treatments

AgNPs were prepared as previously described (Vila et al., 2018). After the cells' differentiation, the apical medium of the cocultures was removed and replaced by 0.5 mL of the selected AgNPs dispersion diluted in DMEM culture medium. The basolateral chamber was replaced with fresh DMEM and the plates were incubated at 37 °C for the desired exposure time.

2.6. Cell viability assay

Cell viability was determined by the Beckman counter method with a ZTM Series coulter-counter (Beckman Coulter Inc., USA). This study was carried out to select the doses to be used in the experiments. Briefly, the differentiated Caco-2 and HT29 cells were exposed to AgNPs for 24 h at the following concentrations: 0, 10, 25, 75, 100, and 150 μg/mL. After the exposure time, the monolayers were washed twice with PBS for 5 min and detached with trypsin-EDTA 1% by incubating the cells at 37 °C for 5 min. The detached cells were diluted 1/100 in ISOTON and counted with a Beckman Cell Counter. The obtained percentage values constitute an average of the number of cells of each treatment compared to the untreated control cultures.

2.7. Paracellular permeability assessment

The barrier's permeability was analyzed by measuring the paracellular transport of Lucifer yellow (LY) (ThermoFisher Scientific, USA). After the given exposure time/concentration, the Transwells® were washed three times with transport buffer (Hank's balanced salt solution, HBSS), Ca^{2+}, Mg^{2+}, 10 mM HEPES [4-(2-hydroxyethyl)-1-piperazineethanesulfonic acid, pH 7.4], and transferred to a new 12-well plate containing 1.5 mL of HBSS in the basolateral compartment. 0.5 mL of a Lucifer yellow solution at 0.4 mg/mL diluted in HBSS was added to the apical compartment. Cells were then incubated for 2 h at 37 °C and, subsequently, 100 μL duplicates of each basolateral chamber were added to a black 96-well plate. Fluorescence was measured at 405–535 nm as excitation-emission spectrum with a fluorimeter (Victor III, Perkin Elmer, USA). As a positive control, cells were treated with 20 mg/mL of benzalkonium chloride for 40 min.

2.8. Assessment of the translocation through the monolayer by ICP-MS

To ascertain the translocation of AgNPs through the *in vitro* barrier model over time, the apical, barrier and basolateral compartments were analyzed separately by Inductively Coupled Plasma-Mass Spectrometry (ICP-MS). After AgNPs exposure, the medium of the apical compartments was collected and transferred to a glass tube. The total medium of the basolateral compartments was resuspended and collected in a separate tube. To collect the membrane compartment, the cells were washed twice with PBS and incubated with 200 μL of trypsin 1% for 5 min at 37 °C. After the incubation time, trypsin was inactivated with 400 μL of trypsin inactivator (FBS 2%). The total volume of cell suspension was collected in a glass tube. All samples were then digested in HNO_3 at 150 °C for 30 min. The amount of AgNPs present in each of the different tubes was determined using an Inductively Coupled Plasma-Mass Spectrometry 7500ce device (Agilent Technologies).

2.9. Cellular localization of AgNPs using confocal microscopy

To assess the localization throughout time of AgNPs in our *in vitro* barrier model, laser confocal microscopy was used. After the barrier's differentiation and AgNPs exposure, the barriers were stained for

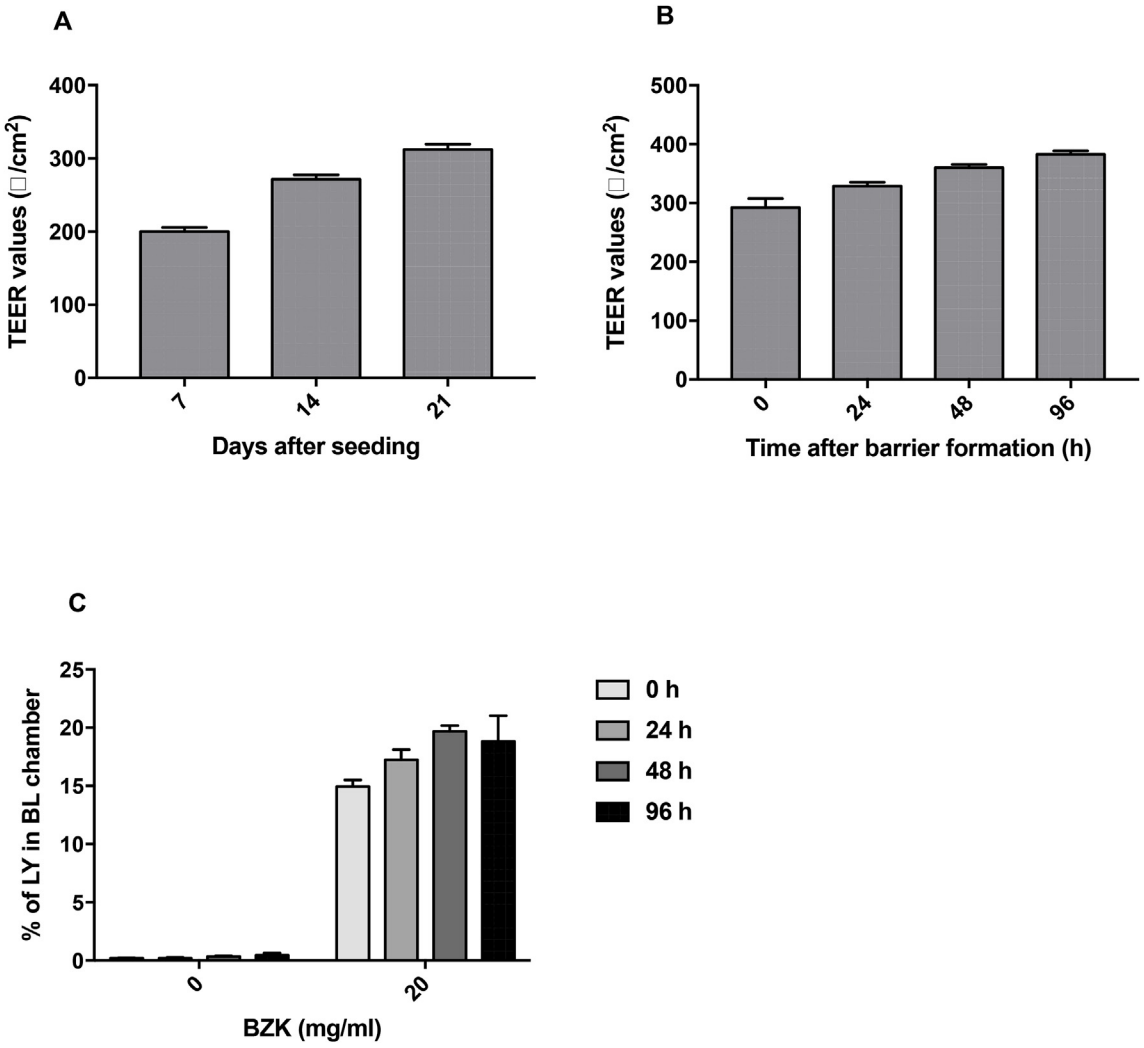

Fig. 2. GIB model stability analysis during and after differentiation. (A) TEER values evaluated 7, 14, and 21 days after seeding. (B) TEER values measured after 0, 24, 48, and 96 h after the barrier's formation (day 21st). (C) Percentage of Lucifer yellow in the basolateral chamber after 0, 24, 48 and 96 h after the barrier's formation. Benzalkonium chloride (BZK, 20 mg/mL) was used as positive control. All data are represented as mean ± SEM.

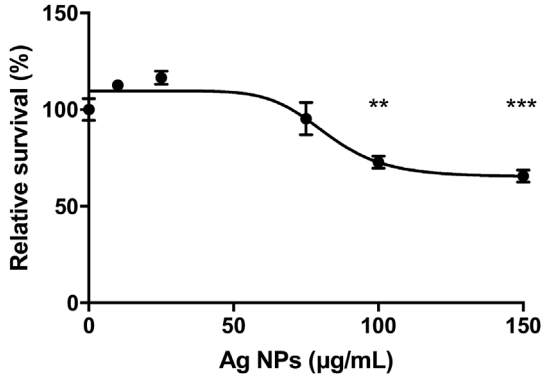

Fig. 3. Relative survival of Caco-2/HT29 differentiated co-culture after 24 h of exposure to AgNPs at concentrations ranging from 0 to 150 µg/mL. Data are represented as the percentage of counted cells compared to the untreated control ± SEM. All data are represented as mean ± SEM and analyzed by one-way ANOVA and Dunnett's multiple comparisons test (**$P < 0.01$; (***$P < 0.001$).

15 min at room temperature. The nucleus was stained with Hoechst 33342 diluted 1:500 (ThermoFisher Scientific, USA), and the mucus was dyed with Wheat Germ Agglutinin, Alexa FluorTM 633 Conjugate (WGA) (ThermoFisher Scientific, USA) diluted 1:100. Both fluorophores were diluted in DMEM cell culture medium. AgNPs were visualized thanks to their capacity to reflect light. AgNPs were manually masked in green, the nuclei in blue and the mucus layer in red. After staining, the monolayers were washed twice with DMEM, the membrane was cut using a scalpel and placed in Glass Bottom Microwell Dishes (MatTek, USA) with 25 µL of mounting medium to maintain the cell's integrity and homeostasis. Sample images were acquired using a Leica TCS SP5 confocal microscope, processed with Huygens essential 4.40p6 (Scientific Volume Imaging, Netherland) and, finally, modified with the Imaris 8.2.1 software (Bitplane, AG).

2.10. Gene expression studies by real-time RT-PCR

Total RNA was extracted using TRIzol® Reagent (Sigma-Aldrich, Germany) following the manufacturer's instructions. To discard residual DNA contamination, the samples were treated with RNase-free DNase I (Turbo DNA-free kit; Invitrogen, USA). 100 ng/µL of total RNA were then used to obtain the cDNA by retrotranscription with the High Capacity RNA-to-cDNA kit (Applied Biosystems, USA). The resulting cDNA was analyzed by real-time PCR on a LightCycler-480 to evaluate the relative expression of the different genes. The *Occludin* (*OCLN*), *Claudin* (*CLDN2*), and *Zona occludens* (*ZO-1*) genes, which code for tight-junction components, were analyzed together with *MUC1,* which

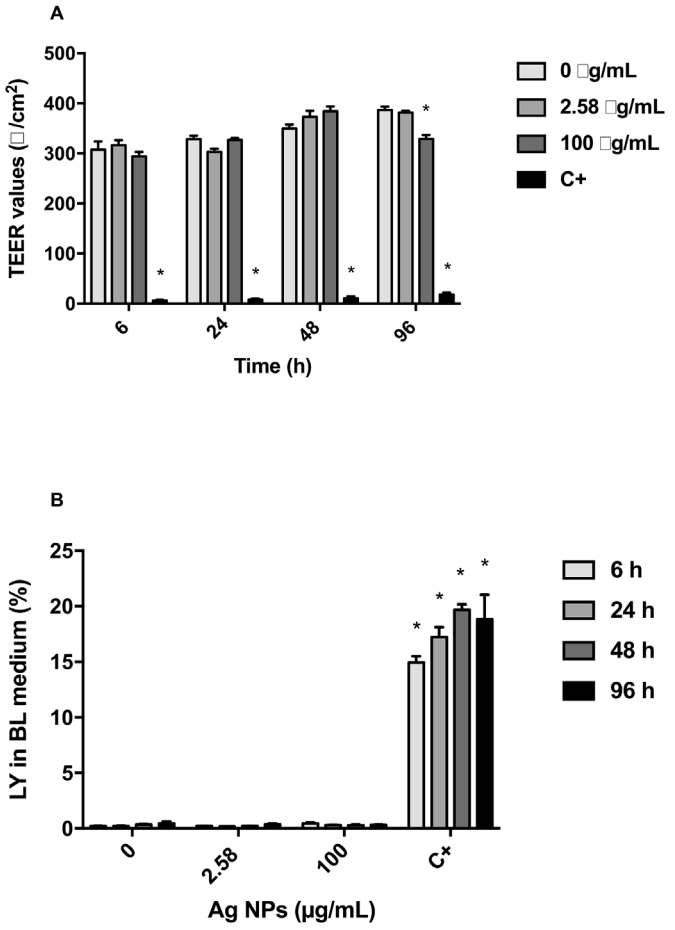

Fig. 4. AgNPs' effects on the barrier's stability. (A) TEER values after the exposure to AgNPs at different time points and concentrations, or BZK 20 mg/mL (C^+) as the positive control. (B) Percentage of Lucifer yellow in the basolateral chamber after AgNPs exposure, or BZK 20 mg/mL (C^+). All data are represented as mean ± SEM and analyzed by one-way ANOVA and Dunnett's multiple comparisons test (*$P < 0.001$). Statistical analysis compared each treatment to its time-matched untreated control.

was also selected as a *mucin-coding* gene. The housekeeping control used was the *ß-Actin* gene.

A total volume of 10 µL per RT-PCR reaction was analyzed, containing 30 ng of cDNA, 5 µL of Light Cycler 480 SYBR Green I Mater (Roche, Germany), 1 µL of H_2O and 1 µL of each primer at 10 µM. The cycling parameters were the following: an initial step of 95 °C for 5 min, then 45 cycles of 95 °C for 10 s, 62 °C or 65 °C for 15 s, and 72 °C for 25 s. Cycle time (Ct) values were obtained with the Light Cycler 480 software package and then normalized with β-Actin Ct values.

2.11. Statistical analysis

All samples and their corresponding measurements were performed in duplicates in three independent experiments. The results are expressed as mean ± SEM. One-way ANOVA with Tukey's post hoc test, unpaired Student's t-test, or two-way ANOVA were used as convenient using GraphPad Prism version 7.00 for Mac (GraphPad Software, San Diego California USA, www.graphpad.com). In all cases, differences were considered significant at p-value of $P < 0.05$.

3. Results

3.1. AgNPs characterization

TEM was used to characterize both the morphology and agglomeration status of the AgNPs used. As indicated in Fig. 1A, the obtained images show that AgNPs had a spherical morphology with an average diameter of 4.84 ± 2.1 nm, as assessed by measuring over 200 particles in random fields of view. Fig. 1B shows the average hydrodynamic radius and zeta potential of a 50 µg/mL AgNPs dispersion in water, which were 9.720 ± 1.571 nm and −20.14 ± 0.611 mV, respectively.

3.2. Integrity of the co-culture barrier

Initially, we assessed the correct formation of the GIB model by measuring TEER values at days 7, 14 and 21 after seeding. As shown in Fig. 2A, there was a progressive increase of TEER values: the highest value was measured at day 21, reaching a mean value of 330.5 ± 16.26 Ω/cm^2.

As our aim was to verify if the Caco-2/HT29 coculture was able to maintain its appropriate barrier function for at least 96 h after the barrier formation, TEER values were monitored 6, 24, 48 and 96 h after the 21st day. Fig. 2B shows a slight increase over time of the obtained TEER values, suggesting a continued cell growth that did not alter the barrier function.

To confirm the results obtained with TEER measurements, the barrier's permeability was also evaluated 6, 24, 48 and 96 h after the 21st day by using the Lucifer yellow assay. As observed in Fig. 2C the fluorophore was unable to cross the barrier, suggesting that the integrity of tight junctions between cells is maintained throughout time.

3.3. Cytotoxicity assessment of AgNPs over time

To evaluate the cytotoxic effects of AgNPs, a viability assay was carried out using exposure doses that ranged from 1 to 150 µg/mL. As shown in Fig. 3, the Caco-2/HT-29 barrier presented a high cytotoxicity resistance to AgNPs exposure. Doses up to 25 µg/mL were unable to induce detectable toxicity. However, concentrations ranging from 25 to 150 µg/mL showed a dose-dependent decrease in the number of counted cells. In the case of 150 µg/mL, the highest concentration tested, the relative survival was around 65%. Considering these results, we selected two concentrations for further experiments: a low concentration of 2.58 µg/mL, which represents the *in vitro* extrapolation of the daily intake of silver nanoparticles estimated by the World Health Organization, and a high dose of 100 µg/mL, which resulted slightly cytotoxic.

3.4. Integrity of the barrier model in response to AgNPs exposure over time

To assess the effects of AgNPs on the barrier's integrity over time, TEER values were monitored throughout the overall length of the experiment. The TEER results for differentiated Caco-2/HT29 exposed to AgNPs over time are shown in Fig. 4A. As observed, TEER values did not change significantly, with the exception of the highest concentration at the longest exposure time, suggesting that the integrity of the barrier was not strongly affected after AgNPs exposure, even after 96 h. Conversely, the exposure to 20 mg/mL of benzalkonium chloride, a well-known barrier disruptor, severely decreased the TEER values of the positive control, implying that the system was able to detect changes in transepithelial electrical resistance.

To confirm these results, the barrier's permeability was evaluated by using the Lucifer yellow assay. As shown in Fig. 4B, the amount of Lucifer yellow that was able to cross the barrier does not change significantly at any dose or exposure time when compared to the untreated control, as opposed to the positive control. Taken together, these results

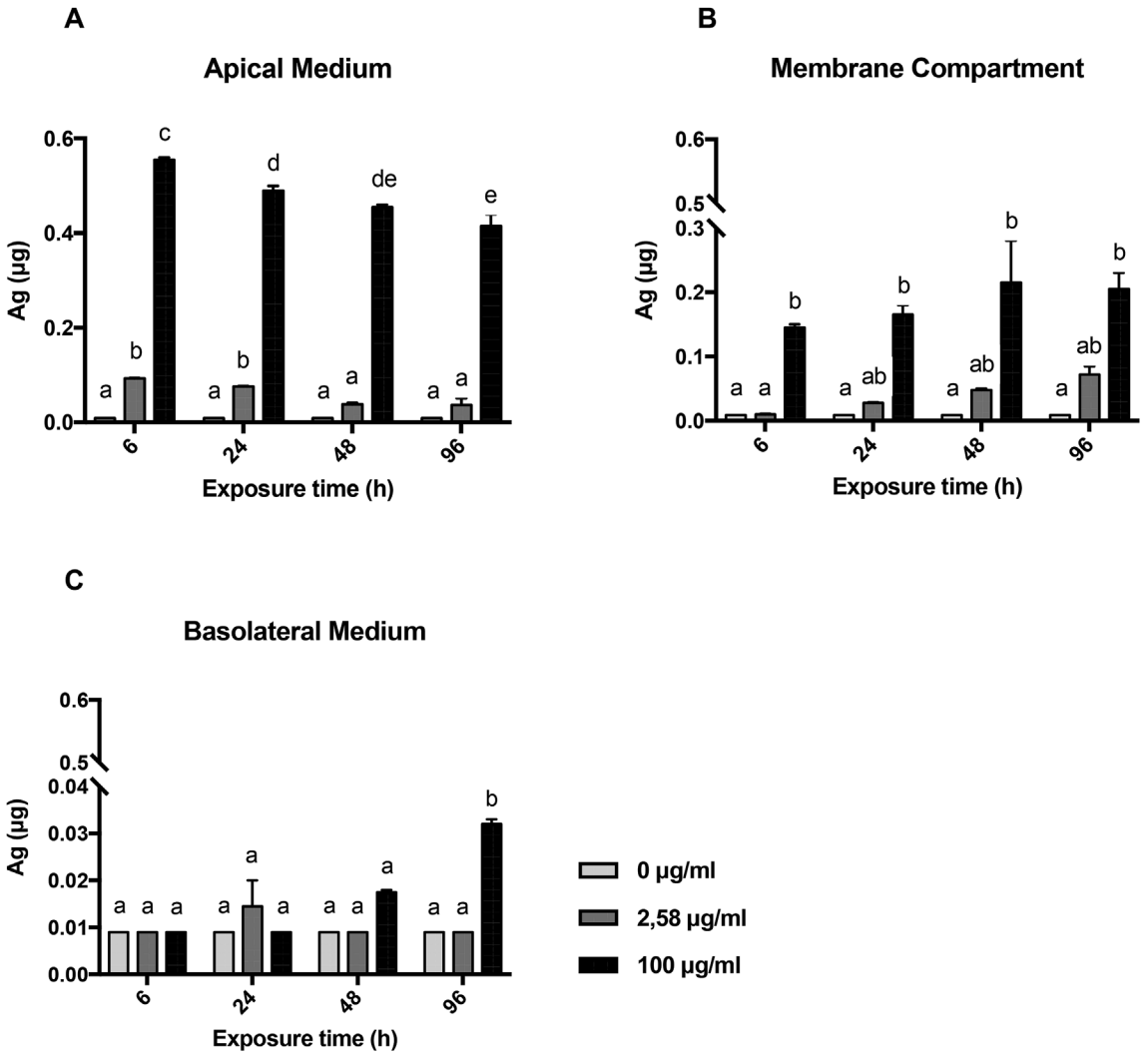

Fig. 5. ICP-MS quantitation of total Ag in the apical (A), membrane (B), or basolateral compartment (C) after 6, 24, 48 and 96 h of AgNPs exposure at 2.58 and 100 µg/mL. Data are represented as mean ± SEM and were analyzed with Two-way ANOVA and a Tukey's post-test. Bars with different letters show statistically significant differences (*$P < 0.05$).

indicate that AgNPs exposure does not destabilize our barrier model under the analyzed conditions.

3.5. Localization of AgNPs in the different compartments

To assess whether AgNPs were able to cross the GIB model after 96 h, we analyzed the amounts of Ag in the apical, cells monolayer, and basolateral compartments after different time points by using ICP-MS. The obtained results for each one of the compartments are indicated in Fig. 5.

As shown in Fig. 5A, there was a tendency to decrease the amount of Ag in the apical medium over time. This could be due to the fact that AgNPs deposit on the cell membrane, are uptake by the cells, or crossed through the barrier. In Fig. 5B, we could observe that the lowest concentration showed a tendency to increase the amount of Ag associated with the cells monolayer over time. However, this was not the case for the highest concentration, which seemed to arrive at its saturation point already at 6 h. Finally, the basolateral medium (Fig. 5C) showed that no significant translocation of silver occurs at the lowest concentration, independently of the exposure time. On the contrary, the transwells exposed to the highest concentration exhibited significant increases of Ag in the basolateral compartment at exposures lasting 48 and 96 h. In this case, most of the values were higher than 0.01 µg, which corresponds to the detection limit of the method. These results point out that AgNPs are able to translocate through our barrier model.

3.6. AgNP uptake and internalization detected by confocal microscopy

As we were able to observe a time-dependent tendency to increase the amount of Ag in the barrier compartment for at least one of the concentrations tested, confocal microscopy was used to get information regarding the behaviour and localization of AgNPs inside the barrier structure. Representative images of our findings can be seen in Figs. 6–8. As observed, we were able to detect changes regarding the nanoparticles localization depending on the exposure time and concentration used. After 24 h of exposure, most of the AgNPs were embedded into the apical mucus layer (Fig. 6B and C). At 48 h (Fig. 7B and C), AgNPs were already uptake by the cells and localized inside/close to the nuclei or between cells, independently of the concentration used. Finally, in Fig. 8, which corresponds to the 96 h exposure, a higher amount of AgNPs was able to cross the mucus barrier and enter the cells. These results suggest that there is a time-dependent increase in cellular uptake and internalization after AgNPs exposure.

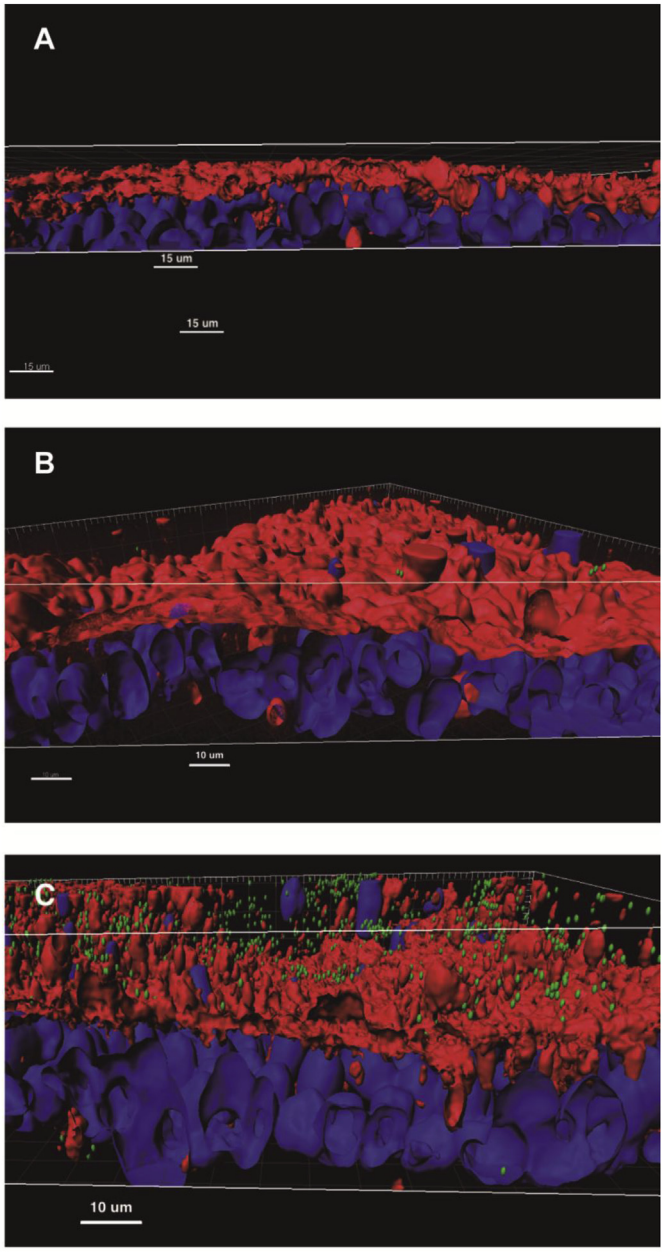

Fig. 6. Three-dimensional images acquired with confocal microscopy of the Caco-2/HT29 coculture barrier model after 24 h of exposure to AgNPs. The nuclei (blue) were stained with Hoechst and the mucus shed (red) was stained with WGA. AgNPs are visualized in green. (A) Untreated control, (B) 2.58 μg/mL, and (C) 100 μg/mL. (For interpretation of the references to color in this figure legend, the reader is referred to the Web version of this article.)

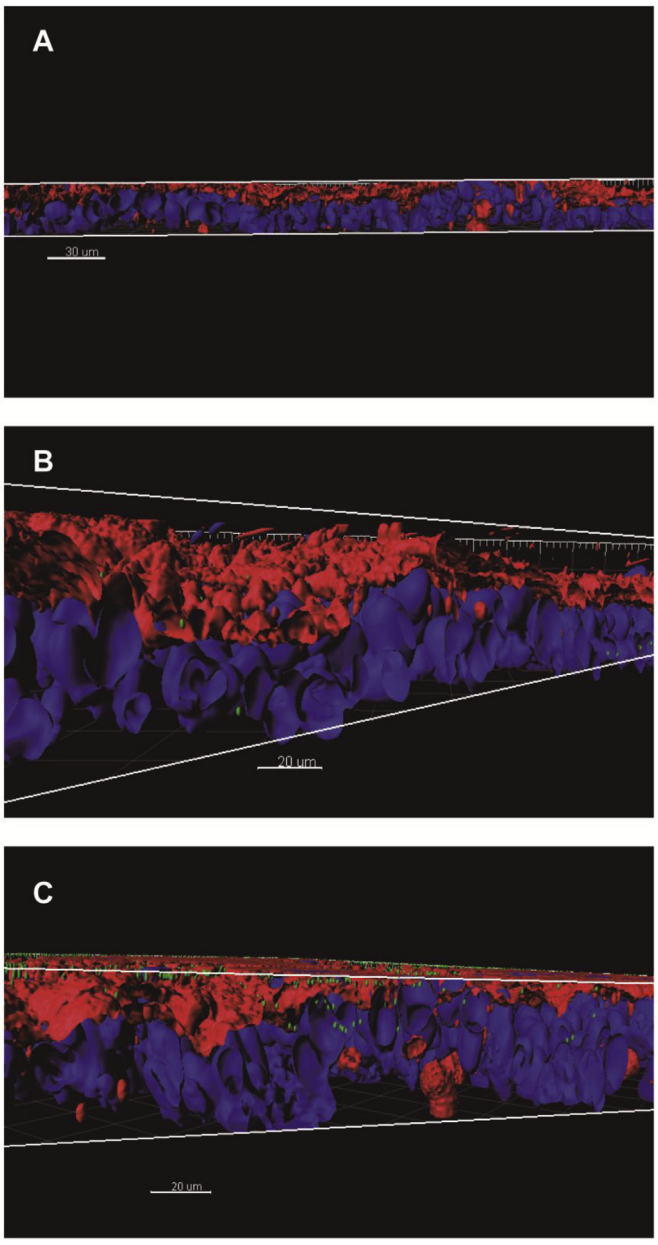

Fig. 7. Three-dimensional images acquired with confocal microscopy of the Caco-2/HT29 coculture barrier model after 48 h of exposure to AgNPs. The nuclei (blue) were stained with Hoechst and the mucus shed (red) was stained with WGA. AgNPs are visualized in green. (A) Untreated control, (B) 2.58 μg/mL, and (C) 100 μg/mL. (For interpretation of the references to color in this figure legend, the reader is referred to the Web version of this article.)

3.7. Changes in the expression of molecular markers after AgNPs exposure

As observed in Fig. 9, our results using real-time RT-PCR show a wide variability in the response to AgNPs exposure depending on the gene, the time of exposure and the selected concentration used. A decrease in mRNA expression can be seen for *OCLN*, *ZO-1* and *MUC1* after 24 h of exposure, especially at the highest concentration (Fig. 9 A, C and D). A similar effect can be observed for *CLDN2* at 48 h (Fig. 9B). However, if we take into consideration the final time-point, the genes involved in the formation of tight junctions and mucus production do not seem to change in a significant manner after the AgNPs' exposure, suggesting that AgNPs induce an initial gene expression deregulation that is brought back to normal levels after 96 h.

4. Discussion

The barrier model of Caco-2/HT29 cells coculture has been proposed as a useful *in vitro* model because it better mimics the intestinal epithelium characteristics when compared to the Caco-2 monolayer (Sahu, 2016; Lozoya-Agullo et al., 2017). However, most of the *in vitro* studies that evaluate the effects of ingested nanomaterials use short exposure times (Martirosyan et al., 2014; Akbari et al., 2017; Ude et al., 2017), underestimating the potential time-dependent cumulative effects of NPs exposure. Thus, we decided to analyze the usefulness of the complex Caco-2/HT29 barrier model up to 96 h, in order to carry out longer exposure studies. AgNPs were selected due to their extensive use in consumer products (McShan et al., 2014). Furthermore, two different AgNPs concentrations were analyzed: one that resulted slightly

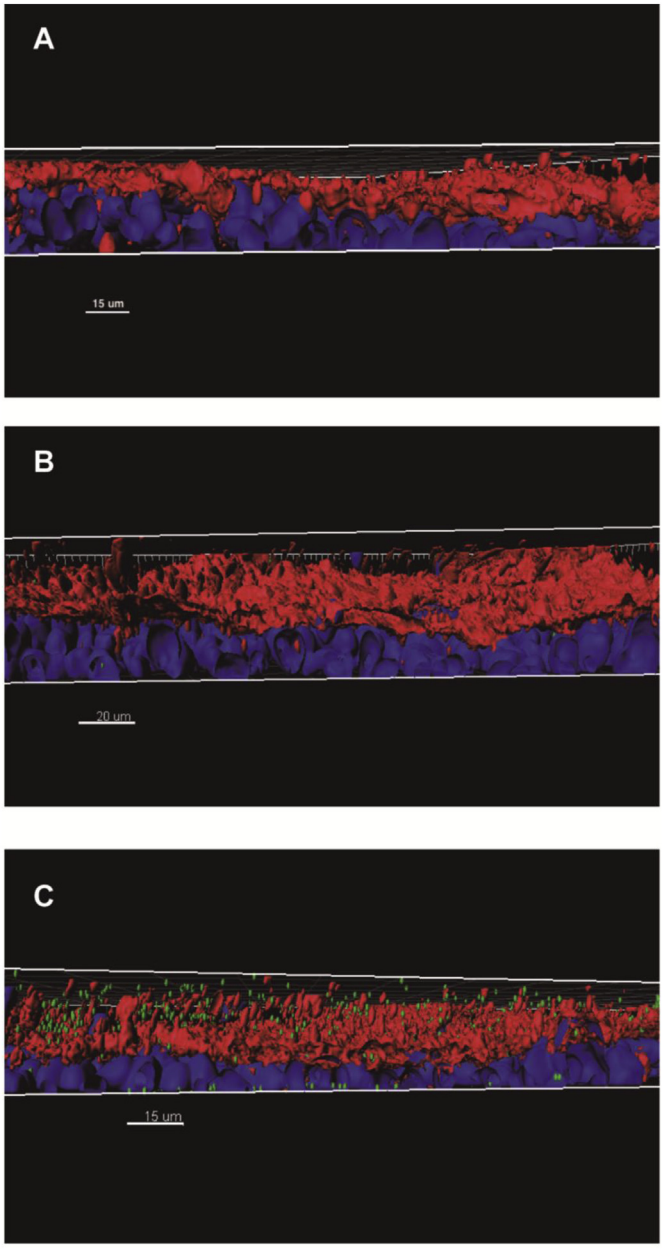

Fig. 8. Three-dimensional images acquired with confocal microscopy of the Caco-2/HT29 coculture barrier model after 96 h of exposure to AgNPs. The nuclei (blue) were stained with Hoechst and the mucus shed (red) was stained with WGA. AgNPs are visualized in green. (A) Untreated control, (B) 2.58 μg/mL, and (C) 100 μg/mL. (For interpretation of the references to color in this figure legend, the reader is referred to the Web version of this article.)

cytotoxic (100 μg/mL), and one that represented the *in vitro* extrapolation of the daily intake of AgNPs estimated by the World Health Organization (2.58 μg/mL). For this estimation, only the first section of the intestine was considered, as this is where most part of the absorption of ingested material occurs. This section has an absorbing area around 900 cm^2 (García-Rodríguez et al., 2018). Knowing that the daily amount of AgNPs intake is 20–80 μg/day, the small intestine's epithelium is exposed to approximately 88.8 g/cm^2 (Fröhlich and Fröhlich, 2016). As the transwells' surface area is 1.12 cm^2, assuming an enlargement factor of 13 times due to microvilli surface, and knowing that the volume of cell culture medium in the apical compartment is 0.5 mL, we determined that the final concentration should be around 2.58 μg/mL.

Our results show for the first time that the integrity of the barrier remains intact even after exceeding the 21 days required for the barrier's proper formation, as corroborated by TEER values and the sustained block of LY paracellular translocation. These results suggest that this model is solid enough to be used for nanoparticles hazard assessment using exposures as long as 96 h. When analyzing the potential effects of AgNPs over the barrier's integrity, we were only able to observe a significant variation in TEER values after exposures to 100 μg/mL lasting for 96 h, suggesting that longer exposure times could indeed have a long-term destabilizing effect that is not visible after shorter times of exposure. Conversely, the LY assay showed no changes in the translocation of the fluorophore at any concentration or time of exposure, suggesting that the tight junctions remained intact.

Using ICP-MS to quantify Ag in the different compartments over time, we observed a significant time-dependent decrease of Ag in the apical compartment for both of the concentrations used, which was reflected in an increase in the basolateral compartment, although the amount of Ag translocating through the barrier was only observed after 48 h, and most of the Ag accumulates in the cell membrane. Nonetheless, this technique does not distinguish between ions and NPs, so it is impossible to know how much of the quantified Ag corresponds to AgNPs (Williams et al., 2016). Confocal microscopy was used to overcome this problem, as it allows the visualization of metallic nanoparticles thanks to their intrinsic refraction, albeit not discriminating individual and aggregated nanoparticles (Vila et al., 2017; García-Rodríguez et al., 2018). The images obtained with this technique showed a time-dependent cellular uptake of the AgNPs. Similar uptake results have been obtained with undifferentiated Caco-2 cells (Georgantzopoulou et al., 2016; Vila et al., 2017), however, our model allows the exact localization of the uptake AgNPs in the different membrane compartments. Although the number of nanoparticles observed inside the cytoplasm and nucleus increased with time, most of the particles were retained in the mucus shed, confirming that this protective barrier impedes the cellular internalization of AgNPs. These results, together with the low paracellular transport of LY in the membrane permeability assay, lead us to hypothesize that the main translocation route of AgNPs is transcytosis, and that its detection is possible only after long-time exposures, reaffirming the idea that longer exposure times allow us to understand better the kinetics of nanomaterials-barrier interactions, as other authors have previously suggested (Gehrke et al., 2011; Joshi et al., 2014; Imai et al., 2017).

By analyzing the transcriptional response to AgNPs over time, we could detect a large variability in mRNA expression levels. More importantly, the analysis of the 24 h time point shows a significantly different scenario when compared to the 96 h treatment. In the first time point, *OCLN*, *CLDN2*, *ZO-1 and MUC1* present gene expression deregulation at one or both doses, suggesting a stronger response to AgNPs. However, as it occurred with the rest of the end-points analyzed in this study, results point out that this deregulation normalizes after 96 h. One explanation could be the barrier's composition, as Caco-2 cells could respond to AgNPs-induced stress in a different manner than HT29 cells. Also, the heterogeneity in differentiation stages of both cell types' cellular subpopulations could also determine the observed transcriptional variability. In spite of this, the overall gene expression changes observed indicate that AgNPs affect the cells at the molecular level, although further research, such as the transcriptional analysis of each cell type separately, is needed to elucidate the mechanisms underlying these variations.

As a concluding remark, it should be emphasized that the effects caused by AgNPs were observed only due to the increase in the exposure time to 96 h. This reinforces our proposal of expanding exposure times beyond 24 h when performing assays for hazard assessment of NPs, as extending the observation window allows the visualization of hidden effects when analyzing shorter exposures. As the use of nanoparticles is expected to increase in the near future, as well as their constant, long-term contact with the population, the development of *in*

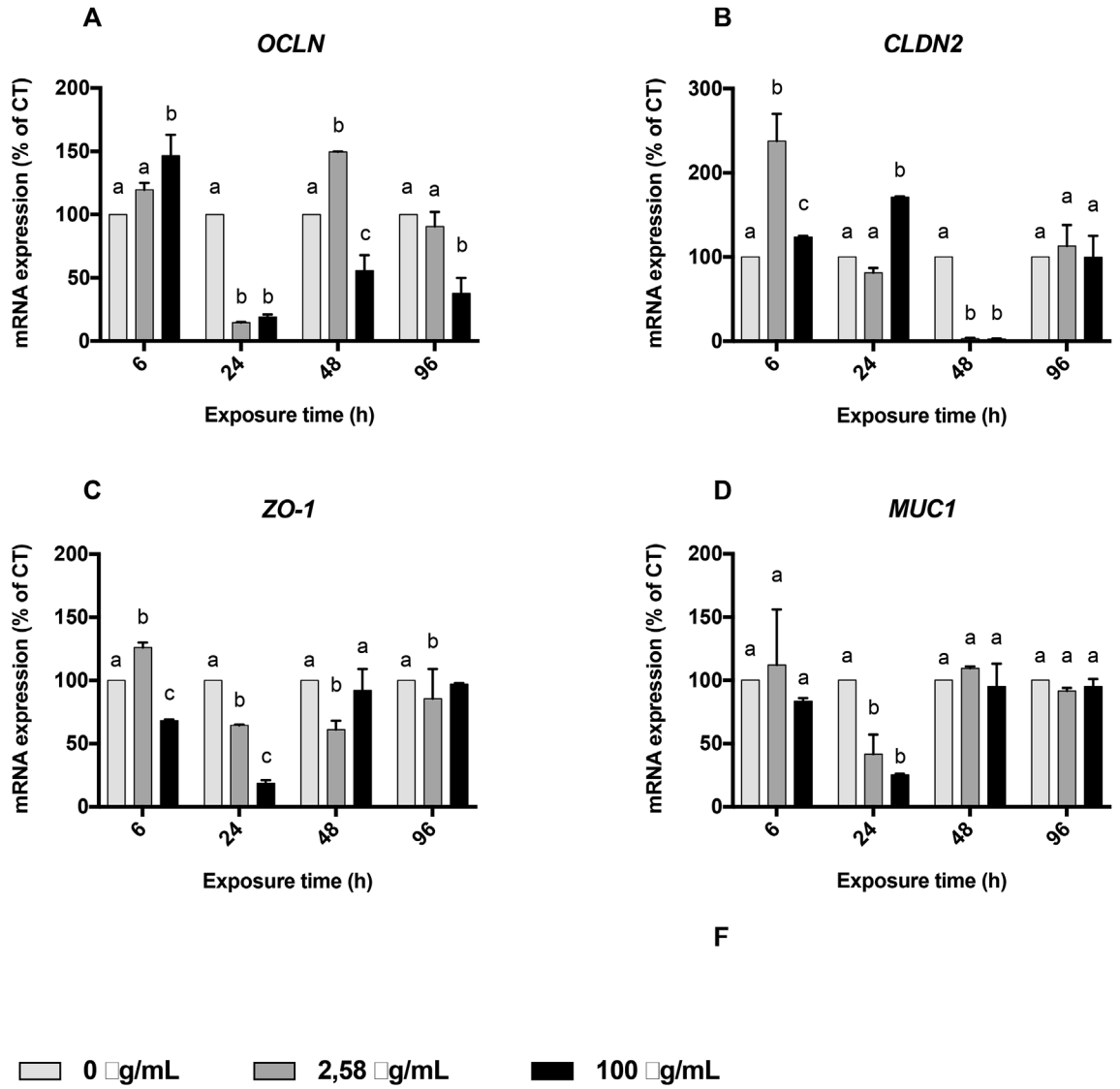

Fig. 9. Relative mRNA expression analysis using real-time RT-PCR of *OCLN* (A), *CLDN2* (B), *ZO-1* (C) and *MUC1* (D) genes of the Caco-2/HT29 coculture barrier model treated with 2.58 μg/mL or 100 μg/mL of AgNPs for 6, 24, 48 and 96 h. Data represented as mean ± SEM and analyzed by the Two-way ANOVA with a Tukey's post-test. Bars with different letters at the same time point show statistically significant differences compared to their time-matched untreated control (*$P < 0.05$).

vitro models for long-term studies is crucial. The results of the present study support that the Caco-2/HT29 coculture is a good candidate model to carry out the aforementioned studies, although determining the barrier's maximum time of endurance after the standard growing period of 21 days could further improve the model's usefulness.

Declaration of interest

The authors report no conflict of interest. The authors alone are responsible for the content and writing of the paper.

Acknowledgements

This investigation has been partially supported by the Ministry of Science, Innovation and Universities (SAF2015-63519-R). J. Domenech and A. Garcia-Rodriguez were funded by postgraduate fellowships from the Universitat Autònoma de Barcelona. We thank Dr Mohamed Alaraby for his help in AgNPs characterization. We would like to thank C. Valiente for his expert technical help.

Transparency document

Transparency document related to this article can be found online at https://doi.org/10.1016/j.fct.2018.11.009.

References

Akbari, A., Lavasanifar, A., Wu, J., 2017. Interaction of cruciferin-based nanoparticles with Caco-2 cells and Caco-2/HT29-MTX co-cultures. Acta Biomater. 64, 249–258.
Annangi, B., Bach, J., Vales, G., Rubio, L., Marcos, R., Hernández, A., 2015. Long-term exposures to low doses of cobalt nanoparticles induce cell transformation enhanced by oxidative damage. Nanotoxicology 9, 138–147.
Brun, E., Barreau, F., Veronesi, G., Fayard, B., Sorieul, S., Chanéac, C., Carapito, C., Rabilloud, T., Mabondzo, A., Herlin-Boime, N., Carrière, M., 2014. Titanium dioxide nanoparticle impact and translocation through ex vivo, in vivo and in vitro gut epithelia. Part. Fibre Toxicol. 11, 13.
Echegoyen, Y., Nerín, C., 2013. Nanoparticle release from nano-silver antimicrobial food containers. Food Chem. Toxicol. 62, 16–22.
Fontdevila, M., Herrer, R., Casallas, M.C., Abecia, L., Ducha, J.J., 2008. Silver nanoparticles as potential antimicrobial additive for weaned pigs. Anim. Feed Sci. Technol. 159, 259–269.
Fröhlich, E.E., Fröhlich, E., 2016. Cytotoxicity of nanoparticles contained in food on intestinal cells and the gut microbiota. Int. J. Mol. Sci. 17, 509.
García-Rodríguez, A., Vila, L., Cortés, C., Hernández, A., Marcos, R., 2018. Effects of

differently shaped TiO_2NPs (nanospheres, nanorods and nanowires) on the *in vitro* model (Caco-2/HT29) of the intestinal barrier. Part. Fibre Toxicol. 15, 33.
Gehrke, H., Pelka, J., Hartinger, C.G., Blank, H., Bleimund, F., Schneider, R., Gerthsen, D., Bräse, S., Crone, M., Türk, M., Marko, D., 2011. Platinum nanoparticles and their cellular uptake and DNA platination at non-cytotoxic concentrations. Arch. Toxicol. 85, 799–812.
Georgantzopoulou, A., Serchi, T., Cambier, S., Leclercq, C.C., Renaut, J., Shao, J., Kruszewski, M., Lentzen, E., Grysan, P., Eswara, S., Audinot, J., Contal, S., Ziebel, J., Guignard, C., Hoffmann, L., Murk, A., Gutleb, A., 2016. Effects of silver nanoparticles and ions on a co-culture model for the gastrointestinal epithelium. Part. Fibre Toxicol. 13, 9.
Halleux, C., Schneider, Y.J., 1991. Iron absorption by intestinal epithelial cells: 1. CaCo2 cells cultivated in serum-free medium, on polyethyleneterephthalate microporous membranes, as an *in vitro* model. In Vitro Cell. Dev. Biol. 27A, 293–302.
Hidalgo, I., 1996. Cultured intestinal epithelial cell models. Pharmaceut. Biotechnol. 8, 35–50.
Iavicoli, I., Leso, V., Fontana, L., Calabrese, E., 2018. Nanoparticle exposure and hormetic dose–responses: an update. Int. J. Mol. Sci. 19, 805.
Imai, S., Morishita, Y., Hata, T., Kondoh, M., Yagi, K., Gao, J.Q., Nagano, K., Higashisaka, K., Yoshioka, Y., Tsutsumi, Y., 2017. Cellular internalization, transcellular transport, and cellular effects of silver nanoparticles in polarized Caco-2 cells following apical or basolateral exposure. Biochem. Biophys. Res. Commun. 484, 543–549.
Johansson, M.E.V., Phillipson, M., Petersson, J., Velcich, A., Holm, L., Hansson, G.C., 2008. The inner of the two Muc2 mucin-dependent mucus layers in colon is devoid of bacteria. Proc. Nat. Acad. Sci. USA 105, 15064–15069.
Joshi, G., Kumar, A., Sawant, K., 2014. Enhanced bioavailability and intestinal uptake of Gemcitabine HCl loaded PLGA nanoparticles after oral delivery. Eur. J. Pharmaceut. Sci. 60, 80–89.
Le Ferrec, E., Chesne, C., Artusson, P., Brayden, D., Fabre, G., Gires, P., Guillou, F., Rousset, M., Rubas, W., Scarino, M.L., 2001. *In vitro* models of the intestinal barrier: the report and recommendations of ECVAM workshop 461,2. Altern. Lab. Anim. 29, 649–668.
Lefebvre, D.E., Venema, K., Gombau, L., Valerio, L.G., Raju, J., Bondy, G.S., Bouwmeester, H., Singh, R.P., Clippinger, A.J., Collnot, E.M., Mehta, R., Stone, V., 2015. Utility of models of the gastrointestinal tract for assessment of the digestion and absorption of engineered nanomaterials released from food matrices. Nanotoxicology 9, 523–542.
Levy, E., Mehran, M., Seidman, E., 1995. Caco-2 cells as a model for intestinal lipoprotein synthesis and secretion. Faseb. J. 9, 626–635.
Lozoya-Agullo, I., Araújo, F., González-Álvarez, I., Merino-Sanjuán, M., González-Álvarez, M., Bermejo, M., Sarmento, B., 2017. Usefulness of Caco-2/HT29-MTX and Caco-2/HT29-MTX/Raji B coculture models to predict intestinal and colonic permeability compared to Caco-2 monoculture. Mol. Pharm. 14, 1264–1270.
Martirosyan, A., Bazes, A., Schneider, Y.J., 2014. *In vitro* toxicity assessment of silver nanoparticles in the presence of phenolic compounds-preventive agents against the harmful effect? Nanotoxicology 8, 573–582.
Martirosyan, A., Grintzalis, K., Polet, M., Laloux, L., Schneider, Y.J., 2016. Tuning the inflammatory response to silver nanoparticles via quercetin in Caco-2 (co-)cultures as model of the human intestinal mucosa. Toxicol. Lett. 253, 36–45.
McShan, D., Ray, P.C., Yu, H., 2014. Molecular toxicity mechanism of nanosilver. J. Food Drug Anal. 22, 116–127.
Nanogenotox. (2011). http://www.nanogenotox.eu/files/PDF/Deliverables/nanogenotox%20deliverable%203_wp4_%20dispersion%20protocol.pdf.
Pontier, C., Pachot, J., Botham, R., Lenfant, B., Arnaud, P., 2001. HT29-MTX and Caco-2/TC7 monolayers as predictive models for human intestinal absorption : role of the mucus layer. J. Pharm. Sci. 90, 1608–1619.
Sahu, S.C., 2016. Altered global gene expression profiles in human gastrointestinal epithelial Caco2 cells exposed to nanosilver. Toxicol. Rep. 3, 262–268.
Scholz, S., Sela, E., Blaha, L., Braunbeck, T., Galay-Burgos, M., García-Franco, M., Guinea, J., Klüver, N., Schirmer, K., Tanneberger, K., Tobor-Kapłon, M., Witters, H., Belanger, S., Benfenati, E., Creton, S., Cronin, M.T., Eggen, R.I., Embry, M., Ekman, D., Gourmelon, A., Halder, M., Hardy, B., Hartung, T., Hubesch, B., Jungmann, D., Lampi, M.A., Lee, L., Léonard, M., Küster, E., Lillicrap, A., Luckenbach, T., Murk, A.J., Navas, J.M., Peijnenburg, W., Repetto, G., Salinas, E., Schüürmann, G., Spielmann, H., Tollefsen, K.E., Walter-Rohde, S., Whale, G., Wheeler, J.R., Winter, M.J., 2013. A European perspective on alternatives to animal testing for environmental hazard identification and risk assessment. Regul. Toxicol. Pharmacol. 67, 506–530.
Schneider, H., Pelaseyed, T., Svensson, F., Johansson, M.E.V., 2018. Study of mucin turnover in the small intestine by in vivo labeling. Sci. Rep. 8, 5760.
Shahare, B., Yashpal, M., 2013. Toxic effects of repeated oral exposure of silver nanoparticles on small intestine mucosa of mice. Toxicol. Mech. Methods 23, 161–167.
Sohal, I.S., O'Fallon, K.S., Gaines, P., Demokritou, P., Bello, D., 2018. Ingested engineered nanomaterials: state of science in nanotoxicity testing and future research needs. Part. Fibre Toxicol. 15, 29.
Sun, H., Chow, E.C., Liu, S., Du, Y., Pang, K.S., 2008. The Caco-2 cell monolayer: usefulness and limitations. Expet Opin. Drug Metabol. Toxicol. 4, 395–411.
Ude, V.C., Brown, D.M., Viale, L., Kanase, N., Stone, V., Johnston, H.J., 2017. Impact of copper oxide nanomaterials on differentiated and undifferentiated Caco-2 intestinal epithelial cells; assessment of cytotoxicity, barrier integrity, cytokine production and nanomaterial penetration. Part. Fibre Toxicol. 14, 31.
Vila, L., Marcos, R., Hernández, A., 2017. Long-term effects of silver nanoparticles in caco-2 cells. Nanotoxicology 11, 771–780.
Vila, L., García-Rodríguez, A., Cortés, C., Marcos, R., Hernández, A., 2018. Assessing the effects of silver nanoparticles on monolayers of differentiated Caco-2 cells, as a model of intestinal barrier. Food Chem. Toxicol. 116, 1–10.
Williams, K.M., Gokulan, K., Cerniglia, C.E., Khare, S., 2016. Size and dose dependent effects of silver nanoparticle exposure on intestinal permeability in an *in vitro* model of the human gut epithelium. J. Nanobiotechnol. 14, 62.